Letter

Entropy production and thermodynamic inference for stochastic microswimmers

Michalis Chatzittofi,[1] Jaime Agudo-Canalejo,[1,2,*] and Ramin Golestanian[1,3,†]

[1]*Department of Living Matter Physics, Max Planck Institute for Dynamics and Self-Organization (MPI-DS), D-37077 Göttingen, Germany*

[2]*Department of Physics and Astronomy, University College London, London WC1E 6BT, United Kingdom*

[3]*Rudolf Peierls Centre for Theoretical Physics, University of Oxford, Oxford OX1 3PU, United Kingdom*

(Received 23 October 2023; accepted 9 May 2024; published 21 May 2024)

The question of characterization of the degree of nonequilibrium activity in active matter systems is studied in the context of a stochastic microswimmer model driven by a chemical cycle. The resulting dynamical properties and entropy production rate unravel a complex interplay between the chemical and the hydrodynamic degrees of freedom beyond linear response, which is not captured by conventional phenomenological approaches. By studying the precision-dissipation trade off, a new protocol is proposed in which microscopic chemical driving forces can be inferred experimentally. Our findings highlight subtleties associated with the stochastic thermodynamics of autonomous microswimmers.

DOI: 10.1103/PhysRevResearch.6.L022044

Understanding entropy production and thermodynamic inference [1] in autonomous systems [2], such as stochastic motors [3,4] and microswimmers [5], is of fundamental importance to the study of biological and synthetic active matter [6–9]. These systems typically produce net motion or mechanical work as a consequence of the dissipation of some form of locally available energy (e.g., ATP hydrolysis) [10–12]. A common assumption in the literature is that the dissipation can be quantified by representing the autonomous self-propulsion via an effective external "active force" [8,13–16].

The thermodynamic uncertainty relation (TUR) and its various generalizations quantify the trade off between the precision of a nonequilibrium current and its associated dissipation, and thus provide a powerful tool to infer the underlying driving forces of a system from experimental measurements of its trajectories [1,17–19]. However, many of the models studied until now to test the behavior of TURs have been based on the assumption of tight coupling between chemical and spatial degrees of freedom (where, e.g., a chemical reaction always corresponds to a mechanical step and vice versa) so that the dynamics is effectively one-dimensional, and, hence, rendering the spatial, chemical, and entropy production currents one and the same [17,20–25].

While convenient, these two (related) assumptions are not generally valid. Realistic autonomous swimmers and molecular motors involve at least two distinct currents (e.g., spatial and chemical) and consequently at least two distinct kinds of driving forces. In fact, the relevant coupling in these systems is off diagonal (in the language of linear irreversible thermodynamics [26–28]), as chemical forces drive motion. This is particularly evident in the case of microswimmers, where the force-free constraint on their self-propulsion mechanisms introduces additional complexities [29–36], and has important consequences on the bounds on entropy production [37,38]. A multidimensional version of the TUR (MTUR) can, in principle, be used in multicurrent systems to obtain much-improved bounds on the entropy production, and thus better inference of the underlying driving forces [39]. However, how to exploit this bound in practice is unclear, as typically only the spatial current is measurable, while the chemical current is not. To shed light on the inner workings of autonomous swimmers and motors, we must therefore understand how spatial and chemical forces and currents couple to each other arbitrarily far from equilibrium, beyond linear response.

In this Letter, we study a stochastic three-sphere swimmer [32] as a minimal model that includes both chemical and spatial (hydrodynamic) degrees of freedom; see Fig. 1. The chemical cycle is represented by a four-state process where each state corresponds to a different conformation of the swimmer [Fig. 1(a)]. The key hydrodynamic degree of freedom corresponds to the spatial position of the swimmer, to which an external force may also be applied. The total chemical energy ε associated with a cycle and the external force F are the two affinities that drive the system out of equilibrium and cause the overall swimming [Fig. 1(b)]. From a hydrodynamic derivation (see Appendix A and [40]), we show that the entropy production rate (EPR) can be written as

$$T\dot{\sigma} = J(\varepsilon, F)\varepsilon + V(\varepsilon, F)F, \tag{1}$$

where $J(\varepsilon, F)$ is the chemical current (rate) of the internal cycle (see Fig. 1(b) and [40]) and $V(\varepsilon, F)$ is the velocity of the swimmer. Superficially, Eq. (1) appears to have the standard form of an EPR, with the chemical current J driven by the

*j.agudo-canalejo@ucl.ac.uk
†ramin.golestanian@ds.mpg.de

Published by the American Physical Society under the terms of the Creative Commons Attribution 4.0 International license. Further distribution of this work must maintain attribution to the author(s) and the published article's title, journal citation, and DOI. Open access publication funded by Max Planck Society.

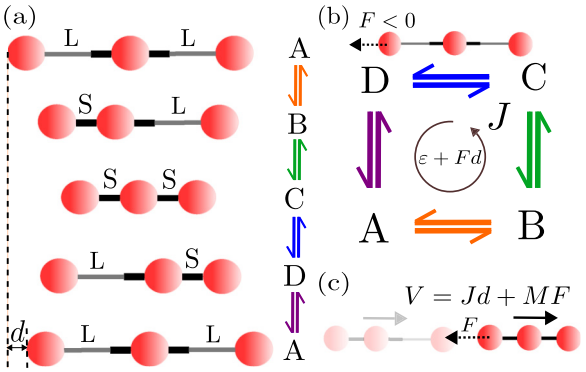

FIG. 1. (a) Full four-state cycle of the stochastic three-sphere swimmer, after which it advances a distance d. L (long) and S (short) indicate the state of the arms. (b) The current J through the cycle is driven by the total affinity $\varepsilon + Fd$, where ε is the chemical affinity and F the external force applied on the swimmer. (c) The total velocity of the swimmer V includes an active swimming contribution Jd and a passive drag MF, with M the hydrodynamic mobility.

chemical affinity ε and the spatial current V driven by the spatial affinity F. However, the hydrodynamics of the swimming mechanism leads to a coupling between the chemical and spatial degrees of freedom, such that the currents J and V do not respectively vanish when ε and F vanish. In fact, we find that the velocity of the swimmer [40] is given by

$$V(\varepsilon, F) = J(\varepsilon, F)d + MF, \tag{2}$$

where the first term represents the active swimming (with d being the distance advanced in the laboratory frame after a full conformational cycle), while the second term is the passive drag of the swimmer by the external force [Fig. 1(c)]. Here, M is the hydrodynamic mobility of the swimmer, which is related to its positional thermal diffusion coefficient through the fluctuation-dissipation relation $D_{\rm th} = Mk_BT$, where k_B is the Boltzmann constant and T is the temperature. Introducing (2) into (1), we can rewrite the EPR as

$$T\dot{\sigma} = J(\varepsilon, F)(\varepsilon + Fd) + MF^2. \tag{3}$$

While perhaps less intuitive, (3) can be viewed as the canonical form of the EPR. Indeed, we show below that the external force influences the dynamics of the chemical cycle through the swimmer mechanics, such that the overall affinity driving the chemical current J is $\varepsilon + Fd$. The passive drag velocity MF in turn represents a hidden current that is exclusively driven by the external force. Therefore, although Eq. (1) is more practical as it involves currents that are observable (at least in principle), it is only when written in the form of Eq. (3) that the nonnegativity of the entropy production rate as required by thermodynamics becomes manifest. Below, we derive these results, and show how they strongly influence the precision-dissipation trade off for the swimmer, and how they can be used to infer the chemical driving force of the swimmer from measurements of its position only.

Model. The model is summarized in Fig. 1(a). We assume quick expansions or contractions of the arms such that their possible states are contracted ($u_\rho = 0$) or expanded ($u_\rho = \delta$), where u_ℓ and u_r represent the deformation of the left and right arms, respectively, and δ is the extension amplitude.

TABLE I. Displacement of each sphere in each transition. For the reverse transitions, $\Delta x_{i,\alpha\beta} = -\Delta x_{i,\beta\alpha}$. The constants $\alpha_{L,S}$ depend on the geometry of the swimmer and satisfy $\frac{1}{3} < \alpha_L < \alpha_S < \frac{1}{2}$. The total displacement d of the swimmer after a full cycle, obtained by summing over any of the columns, is $d = 2(\alpha_S - \alpha_L)\delta$.

Process	$\Delta x_{1,\beta\alpha}/\delta$	$\Delta x_{2,\beta\alpha}/\delta$	$\Delta x_{3,\beta\alpha}/\delta$
$A = LL \longrightarrow B = SL$	$1-\alpha_L$	$-\alpha_L$	$-\alpha_L$
$B = SL \longrightarrow C = SS$	α_S	α_S	$-(1-\alpha_S)$
$C = SS \longrightarrow D = LS$	$-(1-\alpha_S)$	α_S	α_S
$D = LS \longrightarrow A = LL$	$-\alpha_L$	$-\alpha_L$	$1-\alpha_L$

Each conformation corresponds to a state $\alpha = A, B, C, D$ of the chemical cycle. The rate for the transition $\alpha \to \beta$ is denoted as $k_{\beta\alpha}$. The states can also be named based on the arms being long (L) or short (S), e.g., state B corresponds to SL. To introduce forward propulsion (toward the right) without an external force, one must break detailed-balance such that the the trajectory of the system follows closed cycles in the conformational space [30–32]. If the energy released in going from α to β is $\Delta\varepsilon_{\beta\alpha}$, local detailed balance requires $k_{\beta\alpha}/k_{\alpha\beta} = e^{\Delta\varepsilon_{\beta\alpha}/k_BT}$. Note that local detailed balance is required for a thermodynamically consistent definition of stochastic entropy [41]. The total affinity of a cycle is then given by $\varepsilon = \sum \Delta\varepsilon_{\beta\alpha} = k_BT \ln \frac{k_{BA}k_{CB}k_{DC}k_{AD}}{k_{AB}k_{BC}k_{CD}k_{DA}}$. The steady-state probability current J is given by $J = k_{BA}P_A - k_{AB}P_B$, where P_α's are the steady-state probabilities [40]. This current can be viewed as the rate or the inverse period for completion of a chemical cycle. For $\varepsilon = 0$, equilibrium is restored and the current vanishes.

Effect of an external force. We now consider that the swimmer is pulled or pushed by a constant external force F, with the convention that negative force points toward the left (against the direction of swimming). In principle, the force could be distributed among the three spheres such that $F_1 + F_2 + F_3 = F$ where force F_i is applied on the ith sphere. Importantly, the force not only directly drags the swimmer, but also affects its conformational dynamics by modifying the transition rates $k_{\beta\alpha}$. From a hydrodynamic derivation of entropy production (Appendix A), we calculate the total dissipation per transition which includes the work done by the external forces due to the displacements of each sphere.

The displacements $\Delta x_{i,\beta\alpha}$ of the ith sphere during transition $\alpha \to \beta$ are listed in Table I (see Appendix A). Denoting the rates in the absence of the external forces (or the bare rates) as $k_{0\beta\alpha}$, local detailed balance demands that the rates be modified as

$$k_{\beta\alpha} = k_{0\beta\alpha} \exp\left(\frac{\theta_{\beta\alpha}W_{\beta\alpha}}{k_BT}\right), \tag{4}$$

where $W_{\beta\alpha} = \sum_i F_i \Delta x_{i,\beta\alpha}$ is the work done by the external forces. Since the signs of the displacements are reversed in the reverse transitions, this implies that $W_{\alpha\beta} = -W_{\beta\alpha}$. The factors $\theta_{\beta\alpha}$ are related to the location of the energy barrier between states α and β, and must satisfy $\theta_{\alpha\beta} = 1 - \theta_{\beta\alpha}$ [40,42]. Importantly, independently of the choice of $\theta_{\beta\alpha}$ and of where the force is applied, the total affinity of the cycle becomes $k_BT \ln \frac{k_{BA}k_{CB}k_{DC}k_{AD}}{k_{AB}k_{BC}k_{CD}k_{DA}} = \varepsilon + Fd$. Using these ingredients

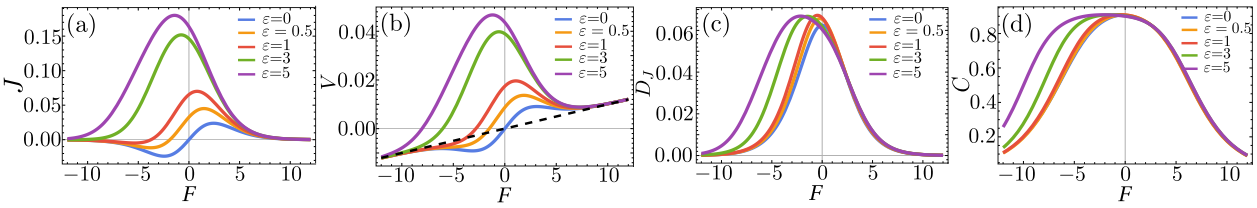

FIG. 2. Dependence on external force F, for several values of the chemical affinity ε, of (a) the chemical current J, (b) the spatial current or velocity V, (c) the chemical diffusion coefficient D_J, and (d) the correlation C between J and V. In (b), the dotted black line represents the passive drag velocity $V = MF$.

and existing results from the literature [43,44] we calculate the chemical current J and its associated diffusion coefficient D_J [40]. Because each conformational cycle results in a displacement $d = 2(\alpha_S - \alpha_L)\delta$ (see Table I), the active swimming contributes Jd to the velocity V of the swimmer, while the force F additionally contributes a passive drift; see Eq. (2). The hydrodynamic mobility M is to the leading order constant during the whole cycle, and more generally, it is an average over all conformations of the swimmer [40]. The spatial diffusion coefficient (associated to V) also includes active swimming and passive hydrodynamic contributions, and reads $D_V = D_J d^2 + D_{\rm th}$ [40]. Using Eq. (2), we can also calculate the correlation between J and V as $C = 1/\sqrt{1 + D_{\rm th}/(D_J d^2)}$ [40].

Swimmer dynamics. In all of the following results, we fix the geometric parameters to $\alpha_L = \frac{2.1}{6}$ and $\alpha_S = \frac{2.9}{6}$; the force is applied on the leftmost (trailing) sphere so that $F_1 = F$ and $F_2 = F_3 = 0$, and we set $\theta_{\beta\alpha} = 1/2$ for all the transitions. The bare transition rates $k_{0\beta\alpha}$ are all set to the same value k, with the exception of k_{0BA} which is set to $k_{0BA} = ke^{\varepsilon/k_BT}$. Furthermore, we focus on strong swimmers and set $D_{\rm th}/k\delta^2 = 10^{-3}$. In all plots, quantities are nondimensionalized using k^{-1} as the timescale, δ as the length scale, and k_BT and k_B as units of energy and entropy, respectively.

Figure 2 displays the behavior of several quantities of interest as a function of the applied force F, for various values of the chemical affinity ε. The chemical current, shown in Fig. 2(a), clearly manifests the mechanochemical coupling in this system, as an applied force can create a chemical current even in the absence of any chemical driving ($\varepsilon = 0$). When $\varepsilon > 0$, the current vanishes at the critical force $F_* = -\varepsilon/d$ that makes the total affinity of the cycle zero, while it is reversed for $F < F_*$. At large positive or negative force, J vanishes [45]. The behavior of the velocity V is similar to that of J [see Fig. 2(b)] except that V shows a linear dependence as $V = MF$ at large force, when it is dominated by the passive drag by the external force since J vanishes. The velocity vanishes at the stall force $F_{\rm s}$, which can be calculated from the implicit equation $J(\varepsilon, F_{\rm s})d + MF_{\rm s} = 0$ [see Eq. (2)] and satisfies $F_* < F_{\rm s} < 0$ (for $\varepsilon > 0$). For sufficiently large ε, small positive forces cause the swimmer to decelerate, whereas small negative forces cause the swimmer to accelerate [32]. This phenomenon, known as negative differential mobility, has also been observed in other nonequilibrium systems [46,47]. Lastly, the force dependence of the chemical diffusion coefficient D_J (which coincides with that of the spatial diffusion D_V, except for a prefactor and a constant baseline) and the correlation C are displayed in Figs. 2(c) and 2(d). We find that both generally peak at small negative values of the applied force, independently of the magnitude of ε.

Entropy production. We can calculate the EPR from the hydrodynamic definition of dissipation, $T\dot\sigma = \sum_i \langle \dot x_i f_i \rangle$, where $\dot x_i$ is the velocity of each sphere and f_i is the corresponding instantaneous force, satisfying the force balance $f_1 + f_2 + f_3 = F$. The crucial step in the derivation is to separately consider the internal and external contributions to the forces (see Appendix A). In this framework, the EPR splits into an active swimming contribution related to the conformational transitions, and a purely passive one. After averaging, these two contributions make up the result presented in Eq. (3). The coupling between chemical and hydrodynamic driving forces gives rise to a rather complicated dependence of the EPR on the forces, with local maxima and minima as shown in Fig. 3(a). For $\varepsilon = F = 0$, the system is at equilibrium. For $\varepsilon > 0$, at low force the entropy production is largely dominated by the chemical part, while at large force we recover the usual hydrodynamic energy dissipation ($\sim F^2$) of a passive object dragged by a constant force.

Thermodynamic precision. The precision of a nonequilibrium process is bounded by the EPR through the TUR [17]. More specifically, the MTUR provides the bound $\boldsymbol{\mathcal{J}}^T \cdot \boldsymbol{\mathcal{D}}^{-1} \cdot \boldsymbol{\mathcal{J}} \leqslant \dot\sigma/k_B$ at steady state, where $\boldsymbol{\mathcal{J}}$ is any vectorial current and $\boldsymbol{\mathcal{D}}$ is the diffusion matrix describing the fluctuations of the current [39]. Applying this bound to the individual current V, we obtain the standard TUR, $V^2/D_V \leqslant \dot\sigma/k_B$. We estimate the quality of this bound using the (nonnegative) factor $Q_V \equiv (V^2/D_V)/(\dot\sigma/k_B)$, which equals one when the bound is saturated and is smaller otherwise. The values of Q_V for our swimmer are shown in Fig. 3(b) as a function of the force F for several values of the chemical driving ε, and in Fig. 3(c) as a function of ε for several values of F. The behavior of Q_V is rather complex, reflecting the fact that the current has two driving forces which can compete with each other.

An intriguing observation can be made by considering the behavior of Q_V near equilibrium ($\varepsilon = F = 0$). While in the limit $F \to 0$ for $\varepsilon = 0$ in Fig. 3(b) we find $Q_V \to 1$ (the bound is saturated), in the limit $\varepsilon \to 0$ for $F = 0$ in Fig. 3(c) we find $Q_V \to 0.8163$ (the bound is not saturated). The two limits do not coincide as one might have naively expected, implying that the near equilibrium limit is not uniquely defined. This generic behavior can be understood in linear response (see Appendix B), and reflects the fact that F is the direct (diagonal) driving force of the current V, whereas ε is its indirect (off-diagonal) driving force [48]. This difference between direct and indirect forces with regards to TUR saturation near equilibrium is of practical relevance, as typically (e.g., for

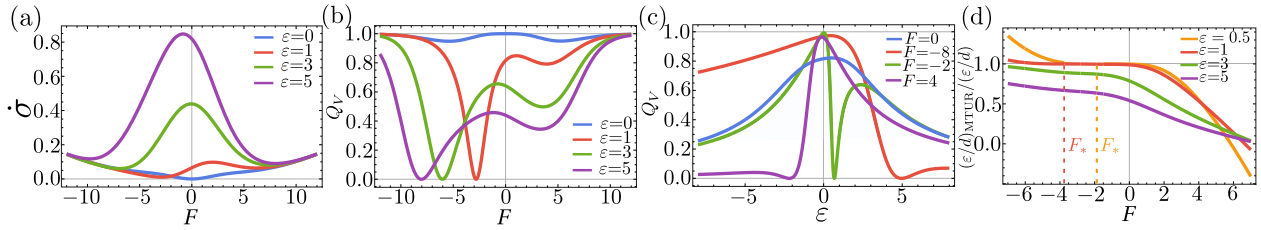

FIG. 3. (a) Entropy production rate $\dot{\sigma}$ as a function of the external force F, for several values of the chemical affinity ε. (b), (c) The quality factor Q_V of the precision-dissipation trade off for the spatial current V, (b) as a function of F for fixed values of ε, and (c) as a function of ε for fixed values of F. (d) Ratio of the MTUR-inferred [Eq. (6)] and true chemical force ε/d. F_* is the critical force at which the chemical current vanishes. For $F > F_*$ the inferred value is a lower bound, for $F < F_*$ an upper bound, and for $F = F_*$ it is exact.

molecular motors and swimmers) the affinity of interest (e.g., ATP hydrolysis) only indirectly drives the measurable current (e.g., spatial velocity).

A tighter bound on entropy production can be obtained by applying the MTUR to the two-dimensional current (J, V), which yields

$$\frac{1}{1-C^2}\left[\frac{J^2}{D_J} - \frac{2CJV}{\sqrt{D_J D_V}} + \frac{V^2}{D_V}\right] \leqslant \frac{\dot{\sigma}}{k_B}. \tag{5}$$

This bound is well behaved and saturated in the near equilibrium limit, as can be proven in the linear response regime (see Appendix B). While it may appear to be less useful in practice, as it involves J, D_J, and C, all of which are not directly observable in an experiment that only has access to the swimmer position, our knowledge of the swimmer mechanics can be exploited to obtain a much improved bound (even an equality) on the chemical energy consumption per unit distance (chemical force) of the swimmer, ε/d.

Thermodynamic inference. Indeed, using Eq. (2) and the expressions for D_V and C, we can write J, D_J, and C as functions of V, D_V, the passive hydrodynamic mobility M (or thermal diffusion coefficient $D_{\rm th} = Mk_BT$), and the external force F; substitute them into (5) together with expression (3) for the EPR; and finally rearrange the terms to obtain an inequality on ε/d. Defining

$$\left(\frac{\varepsilon}{d}\right)_{\rm MTUR} \equiv \frac{k_BTV/D_V - F}{1 - D_{\rm th}/D_V}, \tag{6}$$

we find that, for $F > F_*$ (where $F_* < 0$ is the critical force at which the chemical current vanishes), the MTUR provides a lower bound $\varepsilon/d \geqslant (\varepsilon/d)_{\rm MTUR}$, while for $F < F_*$ the MTUR provides an upper bound $\varepsilon/d \leqslant (\varepsilon/d)_{\rm MTUR}$. By continuity, for $F = F_*$ [which implies $J = 0$ and thus $V = MF_*$ through Eq. (2)], we find the equality $\varepsilon/d = (\varepsilon/d)_{\rm MTUR} = -F_*$. This result is consistent with the total affinity $\varepsilon + Fd$ of the chemical current vanishing at $F = F_*$. The quality of this bound as measured by the ratio $(\varepsilon/d)_{\rm MTUR}/(\varepsilon/d)$ is shown in Fig. 3(d) as a function of F, for several values of ε.

These results reveal several strategies for the inference of the chemical force. In passive measurements with $F = 0$, we can estimate $\varepsilon/d \geqslant k_BT(V/D_V)(1 - D_{\rm th}/D_V)^{-1}$. This improves the bound obtained from the standard TUR by a factor $(1 - D_{\rm th}/D_V)^{-1}$. In active measurements with $F \neq 0$, one may measure the stall force of the swimmer $F_{\rm s} < 0$ at which $V = 0$, as well as the position fluctuations giving D_V, and infer $\varepsilon/d \geqslant -F_{\rm s}(1 - D_{\rm th}/D_V)^{-1}$. Lastly, and optimally, one may measure the critical force F_* at which the swimmer moves precisely at the velocity that one would expect from passive hydrodynamic drag, i.e., $V = MF_*$. The chemical force is then exactly $\varepsilon/d = -F_*$. In all these cases, the passive mobility M (and associated $D_{\rm th} = Mk_BT$) may be estimated from purely hydrodynamic calculations. Alternatively, if $|J(F)|$ grows more slowly than linear, tends to a constant, or vanishes at large force (as is the case for the three-sphere swimmer), M can be measured from the asymptotic behavior of the swimmer velocity as $F \to \pm\infty$; see the force-velocity (F-V) curve in Fig. 2(b). In this case, F_* and thus ε/d can be inferred by measuring the F-V curve, estimating its high-force asymptote, and obtaining the intersection point of the asymptote and the F-V curve, which occurs at F_*.

Discussion. Using a stochastic three-sphere swimmer as an analytically tractable and thermodynamically-consistent model for a chemically powered autonomous microswimmer, we have explicitly calculated its swimming dynamics and its entropy production in the presence of an external force. This allowed us to study the coupling between spatial and chemical forces and currents beyond the linear response regime. We have found a number of interesting properties in the force dependence of the swimmer dynamics as well as its thermodynamic properties, such as the radically different dependence of the thermodynamic precision-dissipation trade off of the swimmer velocity on the external force (direct driving) and internal chemical affinity (indirect driving). Moreover, we have shown how the chemical affinity of the swimmer can be precisely inferred by measurements of the spatial dynamics only.

All of these properties are a consequence of the coupling between spatial and chemical forces and currents in this system, as exemplified by Eqs. (1), (2), (3), and the expressions for D_V and C. Importantly, we expect the form of these equations to remain unchanged for other autonomous swimmers (see, e.g., Ref. [49] for a derivation of equivalent expressions for self-phoretic swimmers). Only the precise functional form of the chemical current $J(\varepsilon, F)$ (and associated diffusion D_J) and the distance d advanced per cycle will depend on the microscopic details. Therefore, the general lessons learned here and the thermodynamic inference strategy proposed [Eq. (6)] should be applicable to a wide range of autonomous motors and swimmers.

Acknowledgments. We acknowledge support from the Max Planck School Matter to Life and the MaxSynBio Consortium which are jointly funded by the Federal Ministry of Education and Research (BMBF) of Germany and the Max Planck Society.

Appendix A: Hydrodynamic calculation of velocity and entropy production. The force balance equation for the swimmer reads $\sum_i f_i = F$. The force on sphere i denoted as f_i can be expressed as $f_i = \tilde{f}_i + F_i$, in terms of the internal force $\tilde{f}_i$ and the external force F_i. We have $\sum_i \tilde{f}_i = 0$ and $\sum_i F_i = F$. The internal forces can be written as $\tilde{f}_1 = -\tilde{f}_\ell$, $\tilde{f}_2 = \tilde{f}_\ell - \tilde{f}_r$, and $\tilde{f}_3 = \tilde{f}_r$, where $\tilde{f}_\ell$ and $\tilde{f}_r$ are respectively the internal stresses on the left and right arms, defined to be positive when they act to expand the arm. We denote the instantaneous speeds of the arms as $\dot{u}_\ell = \dot{x}_2 - \dot{x}_1$, $\dot{u}_r = \dot{x}_3 - \dot{x}_2$. Forces and velocities are linearly related through the hydrodynamic friction tensor Z_{ij} such that $f_i = \sum_j Z_{ij}\dot{x}_j$. By summing over the forces we deduce that $\sum_i A_i \dot{x}_i = BF$, with $A_i(u_\ell, u_r) \equiv (\sum_j Z_{ij})/(\sum_{i,j} Z_{ij})$ and $B(u_\ell, u_r) \equiv 1/(\sum_{i,j} Z_{ij})$. From this expression, we derive equations describing the motion of each of the spheres in response to the external force as well as the changes in the lengths of the arms (active swimming) as follows:

$$\dot{x}_1 = BF - (1 - A_1)\dot{u}_\ell - A_3\dot{u}_r, \tag{A1}$$

$$\dot{x}_2 = BF + A_1\dot{u}_\ell - A_3\dot{u}_r, \tag{A2}$$

$$\dot{x}_3 = BF + A_1\dot{u}_\ell + (1 - A_3)\dot{u}_r. \tag{A3}$$

The average velocity V of the swimmer is given by $\langle \dot{x}_i \rangle$, where the average is taken at steady state and any sphere i may be considered without loss of generality. Choosing $i = 2$, we can write

$$V = \langle \dot{x}_2 \rangle = MF + \langle A_1\dot{u}_\ell - A_3\dot{u}_r \rangle, \tag{A4}$$

where we have defined $M \equiv \langle B \rangle$, which is independent of ε or F to leading order in the hydrodynamic interactions [40]. The first term represents the passive drag, whereas the second term represents the active swimming. The latter results in finite contributions for each conformational change, so that

$$\begin{aligned}\langle A_1\dot{u}_\ell - A_3\dot{u}_r \rangle &= \frac{1}{\mathcal{T}}\int_0^{\mathcal{T}} (A_1\dot{u}_\ell - A_3\dot{u}_r)dt, \\ &= J\sum_{\{\beta\alpha\}}\left[\int_\alpha^\beta A_1 du_\ell - \int_\alpha^\beta A_3 du_r\right], \\ &= J\sum_{\{\beta\alpha\}} \Delta x_{2,\beta\alpha} = Jd,\end{aligned} \tag{A5}$$

where $\mathcal{T} = J^{-1}$ is the period of a cycle in steady state, and the sums run over the forward transitions $\{\beta\alpha\} = \{BA, CB, DC, AD\}$. Equations (A4) and (A5) together result in Eq. (2).

The displacement in each transition $\Delta x_{2,\beta\alpha}$ is calculated by performing the associated integral in the second line of Eq. (A5). For instance, in the transition $A \to B$ the left arm shrinks and the right arm stays fixed at $u_r = \delta$, so that we find

$$\Delta x_{2,BA} = \int_A^B A_1 du_\ell = \int_\delta^0 A_1(u_\ell, \delta)du_\ell = -\alpha_L\delta, \tag{A6}$$

where we have defined

$$\alpha_L \equiv \frac{1}{\delta}\int_0^\delta A_1(u_\ell, \delta)du_\ell. \tag{A7}$$

Conversely, in the transition $B \to C$, the right arm shrinks while the left arm stays fixed at $u_\ell = 0$. We thus find

$$\Delta x_{2,CB} = -\int_B^C A_3 du_r = -\int_\delta^0 A_3(0, u_r)du_r = \alpha_S\delta, \tag{A8}$$

with the definition

$$\alpha_S \equiv \frac{1}{\delta}\int_0^\delta A_3(0, u_r)du_r. \tag{A9}$$

Repeating this procedure for all transitions and calculating the corresponding displacement of the first and third sphere, we obtain the results in Table I, which are valid for a swimmer with symmetric geometry as in Fig. 1. The calculations for a more general asymmetric swimmer, their explicit integration using the Oseen approximation, and the estimation of the bound $1/3 < \alpha_L < \alpha_S < 1/2$ are performed in Ref. [40]. These recover the known results relating the velocity of the swimmer to the area swept by cycles in conformational space [31,32].

To calculate the EPR at steady state, we start from the hydrodynamic dissipation $T\dot{\sigma} = \sum_i \langle \dot{x}_i f_i \rangle$. Using (A1)–(A3), the EPR becomes

$$\begin{aligned}T\dot{\sigma} = MF^2 &+ \langle \dot{u}_\ell[\tilde{f}_\ell - (1 - A_1)F_1 + A_1(F_2 + F_3)] \\ &+ \dot{u}_r[\tilde{f}_r - A_3(F_1 + F_2) + (1 - A_3)F_3]\rangle.\end{aligned} \tag{A10}$$

Here, analogously to the calculation of the velocity, the first term represents the dissipation due to passive drag, whereas the second term represents dissipation due to the active swimming, which gives a finite contribution for each conformational transition.

Indeed, following the same procedure used to derive Eq. (A5), we may write

$$T\dot{\sigma} = MF^2 + J\sum_{\{\beta\alpha\}} T\Delta\sigma_{\beta\alpha}, \tag{A11}$$

where $T\Delta\sigma_{\beta\alpha}$ gives the dissipation occurring during the transition $\alpha \to \beta$. As an example, we consider again the transition $A \to B$. In this transition, u_ℓ shrinks whereas u_r remains constant and fixed to δ. Thus, the discrete dissipation during this transition is

$$\begin{aligned}T\Delta\sigma_{BA} &= \int_\delta^0 [\tilde{f}_\ell - (1 - A_1)F_1 + A_1(F_2 + F_3)]du_\ell \\ &= \Delta\varepsilon_{BA} + F_1\Delta x_{1,BA} + F_2\Delta x_{2,BA} + F_3\Delta x_{3,BA}.\end{aligned} \tag{A12}$$

Here, the first term results from the definition

$$\Delta\varepsilon_{BA} \equiv \int_\delta^0 \tilde{f}_\ell du_\ell, \tag{A13}$$

and gives the dissipation due to the internal active mechanism of the swimmer, while the remaining terms result from the displacements of the spheres previously calculated and give the dissipation by the external force during a conformational change.

An analogous result $T\Delta\sigma_{\beta\alpha} = \Delta\varepsilon_{\beta\alpha} + \sum_i F_i\Delta x_{i,\beta\alpha}$ is obtained for all other transitions [40]. The transition-induced dissipation obtained in this way must be used to enforce local detailed balance in the stochastic transitions, leading to

Eq. (4). Finally, using this result in Eq. (A11), and noting that $\sum_{\{\beta\alpha\}} \Delta\varepsilon_{\beta\alpha} = \varepsilon$ and $\sum_{\{\beta\alpha\},i} F_i \Delta x_{i,\beta\alpha} = Fd$, leads to the expression for the EPR in Eq. (3), which gives Eq. (1) when combined with Eq. (2).

Appendix B: Linear response regime. In the linear-response regime ($\varepsilon, Fd \ll k_BT$), the currents can be written as $J = L_{\varepsilon\varepsilon}\varepsilon + L_{\varepsilon F}F$ and $V = L_{F\varepsilon}\varepsilon + L_{FF}F$, with $L_{\varepsilon\varepsilon} = \tilde{\kappa}$, $L_{FF} = \tilde{\kappa}d^2 + M$, and $L_{\varepsilon F} = L_{F\varepsilon} = \tilde{\kappa}d$, where $\tilde{\kappa} = \kappa_0/(k_BT)$ and κ_0 is an inverse timescale that depends only on the force-free rates $k_{0\beta\alpha}$ [40]. Thus, affinities couple to the currents through $\mathcal{J}_a = \sum_b L_{ab}\mathcal{A}_b$, where $\mathcal{J}_a = (J, V)$ is a vector of currents, $\mathcal{A}_a = (\varepsilon, F)$ is a vector of affinities, and L_{ab} is a symmetric Onsager matrix. The EPR can then be expressed in the usual bilinear form $T\dot{\sigma} = \sum_{ab} L_{ab}\mathcal{A}_a\mathcal{A}_b$ [26–28].

It is straightforward to show that the MTUR ($\boldsymbol{\mathcal{J}}^T \cdot \boldsymbol{\mathcal{D}}^{-1} \cdot \boldsymbol{\mathcal{J}} \leqslant \dot{\sigma}/k_B$) is saturated in linear regime. Indeed, the diffusion matrix $\boldsymbol{\mathcal{D}}$ relates to the Onsager mobility matrix $\boldsymbol{L}$ through the fluctuation-dissipation theorem $\boldsymbol{\mathcal{D}} = k_BT\boldsymbol{L}$, and using this together with $\boldsymbol{\mathcal{J}} = \boldsymbol{L} \cdot \boldsymbol{\mathcal{A}}$ directly results in $\boldsymbol{\mathcal{J}}^T \cdot \boldsymbol{\mathcal{D}}^{-1} \cdot \boldsymbol{\mathcal{J}} = \dot{\sigma}/k_B$. The behavior of the standard single-current TUR, $Q_a \equiv (\mathcal{J}_a^2/D_a)/(\dot{\sigma}/k_B) \leqslant 1$ for current $\mathcal{J}_a$, is more surprising. In general, for a current $\mathcal{J}_a$ driven by N affinities $\mathcal{A}_b$ with $b = 1, \ldots, N$, the quality factor Q_a can be written as

$$Q_a = \frac{\sum_{b,c} L_{ab}L_{ac}\mathcal{A}_b\mathcal{A}_c}{L_{aa}\sum_{b,c} L_{bc}\mathcal{A}_b\mathcal{A}_c}, \tag{B1}$$

where we have used the fluctuation-dissipation relation $D_a = \mathcal{D}_{aa} = k_BTL_{aa}$. There are two distinct cases with regards to how the system behaves when only one of the affinities is nonzero: (i) If $\mathcal{A}_b = 0$ for all $b \neq a$ and $\mathcal{A}_a \neq 0$ (weak direct driving), we find $Q_a = 1$, i.e., the bound saturates; (ii) If $\mathcal{A}_b = 0$ for all $b \neq c$ and $\mathcal{A}_c \neq 0$ for some $c \neq a$ (weak indirect driving), we find $Q_a = L_{ac}^2/(L_{aa}L_{cc})$ [48]. The latter value is guaranteed to be smaller than or equal to one due to the positive semidefiniteness of the Onsager matrix. Typically, it is smaller than one, implying that the TUR bound is not saturated. For our swimmer, we thus have $Q_V \to L_{F\varepsilon}^2/(L_{FF}L_{\varepsilon\varepsilon})$ when $F = 0$ and $\varepsilon \to 0$, which for the parameters used in Fig. 3 gives $Q_V \to 0.8163$.

[1] U. Seifert, From stochastic thermodynamics to thermodynamic inference, Annu. Rev. Condens. Matter Phys. **10**, 171 (2019).

[2] G. Gompper, R. G. Winkler, T. Speck, A. Solon, C. Nardini, F. Peruani, H. Löwen, R. Golestanian, U. B. Kaupp, L. Alvarez, T. Kiørboe, E. Lauga, W. C. K. Poon, A. DeSimone, S. Muiños-Landin, A. Fischer, N. A. Söker, F. Cichos, R. Kapral, P. Gaspard *et al.*, The 2020 motile active matter roadmap, J. Phys.: Condens. Matter **32**, 193001 (2020).

[3] F. Jülicher, A. Ajdari, and J. Prost, Modeling molecular motors, Rev. Mod. Phys. **69**, 1269 (1997).

[4] A.-K. Pumm, W. Engelen, E. Kopperger, J. Isensee, M. Vogt, V. Kozina, M. Kube, M. N. Honemann, E. Bertosin, M. Langecker, R. Golestanian, F. C. Simmel, and H. Dietz, A DNA origami rotary ratchet motor, Nature (London) **607**, 492 (2022).

[5] R. Golestanian and A. Ajdari, Stochastic low reynolds number swimmers, J. Phys.: Condens. Matter **21**, 204104 (2009).

[6] C. Nardini, E. Fodor, E. Tjhung, F. van Wijland, J. Tailleur, and M. E. Cates, Entropy production in field theories without time-reversal symmetry: Quantifying the non-equilibrium character of active matter, Phys. Rev. X **7**, 021007 (2017).

[7] P. Pietzonka and U. Seifert, Entropy production of active particles and for particles in active baths, J. Phys. A: Math. Theor. **51**, 01LT01 (2018).

[8] S. Shankar and M. C. Marchetti, Hidden entropy production and work fluctuations in an ideal active gas, Phys. Rev. E **98**, 020604(R) (2018).

[9] C. Battle, C. P. Broedersz, N. Fakhri, V. F. Geyer, J. Howard, C. F. Schmidt, and F. C. MacKintosh, Broken detailed balance at mesoscopic scales in active biological systems, Science **352**, 604 (2016).

[10] M. L. Mugnai, C. Hyeon, M. Hinczewski, and D. Thirumalai, Theoretical perspectives on biological machines, Rev. Mod. Phys. **92**, 025001 (2020).

[11] S. Borsley, D. A. Leigh, and B. M. W. Roberts, Chemical fuels for molecular machinery, Nat. Chem. **14**, 728 (2022).

[12] R. Golestanian, Phoretic active matter, in *Active Matter and Nonequilibrium Statistical Physics: Lecture Notes of the Les Houches Summer School: Volume 112, September 2018* (Oxford University Press, Oxford, UK, 2022).

[13] T. Speck, Stochastic thermodynamics for active matter, Europhys. Lett. **114**, 30006 (2016).

[14] G. Szamel, Stochastic thermodynamics for self-propelled particles, Phys. Rev. E **100**, 050603(R) (2019).

[15] L. Tociu, E. Fodor, T. Nemoto, and S. Vaikuntanathan, How dissipation constrains fluctuations in nonequilibrium liquids: Diffusion, structure, and biased interactions, Phys. Rev. X **9**, 041026 (2019).

[16] L. Dabelow, S. Bo, and R. Eichhorn, Irreversibility in active matter systems: Fluctuation theorem and mutual information, Phys. Rev. X **9**, 021009 (2019).

[17] A. C. Barato and U. Seifert, Thermodynamic uncertainty relation for biomolecular processes, Phys. Rev. Lett. **114**, 158101 (2015).

[18] T. R. Gingrich, J. M. Horowitz, N. Perunov, and J. L. England, Dissipation bounds all steady-state current fluctuations, Phys. Rev. Lett. **116**, 120601 (2016).

[19] C. Dieball and A. Godec, Direct route to thermodynamic uncertainty relations and their saturation, Phys. Rev. Lett. **130**, 087101 (2023).

[20] P. Pietzonka, A. C. Barato, and U. Seifert, Universal bound on the efficiency of molecular motors, J. Stat. Mech. (2016) 124004.

[21] A. C. Barato and U. Seifert, Cost and precision of brownian clocks, Phys. Rev. X **6**, 041053 (2016).

[22] S. Lee, C. Hyeon, and J. Jo, Thermodynamic uncertainty relation of interacting oscillators in synchrony, Phys. Rev. E **98**, 032119 (2018).

[23] R. Marsland III, W. Cui, and J. M. Horowitz, The thermodynamic uncertainty relation in biochemical oscillations, J. R. Soc. Interface **16**, 20190098 (2019).

[24] T. Koyuk and U. Seifert, Thermodynamic uncertainty relation in interacting many-body systems, Phys. Rev. Lett. **129**, 210603 (2022).
[25] M. P. Leighton and D. A. Sivak, Dynamic and thermodynamic bounds for collective motor-driven transport, Phys. Rev. Lett. **129**, 118102 (2022).
[26] L. Onsager, Reciprocal relations in irreversible processes. I, Phys. Rev. **37**, 405 (1931).
[27] L. Onsager, Reciprocal relations in irreversible processes. II, Phys. Rev. **38**, 2265 (1931).
[28] S. R. De Groot and P. Mazur, *Non-Equilibrium Thermodynamics* (Courier Corporation, North Chelmsford, MA, 2013).
[29] E. M. Purcell, Life at low Reynolds number, Am. J. Phys. **45**, 3 (1977).
[30] A. Najafi and R. Golestanian, Simple swimmer at low Reynolds number: Three linked spheres, Phys. Rev. E **69**, 062901 (2004).
[31] R. Golestanian and A. Ajdari, Analytic results for the three-sphere swimmer at low Reynolds number, Phys. Rev. E **77**, 036308 (2008).
[32] R. Golestanian and A. Ajdari, Mechanical response of a small swimmer driven by conformational transitions, Phys. Rev. Lett. **100**, 038101 (2008).
[33] E. Lauga and T. R. Powers, The hydrodynamics of swimming microorganisms, Rep. Prog. Phys. **72**, 096601 (2009).
[34] R. Golestanian, T. B. Liverpool, and A. Ajdari, Propulsion of a molecular machine by asymmetric distribution of reaction products, Phys. Rev. Lett. **94**, 220801 (2005).
[35] F. Jülicher and J. Prost, Generic theory of colloidal transport, Eur. Phys. J. E **29**, 27 (2009).
[36] P. Gaspard and R. Kapral, Fluctuating chemohydrodynamics and the stochastic motion of self-diffusiophoretic particles, J. Chem. Phys. **148** (2018).
[37] B. Nasouri, A. Vilfan, and R. Golestanian, Minimum dissipation theorem for microswimmers, Phys. Rev. Lett. **126**, 034503 (2021).
[38] A. Daddi-Moussa-Ider, R. Golestanian, and A. Vilfan, Minimum entropy production by microswimmers with internal dissipation, Nat. Commun. **14**, 6060 (2023).
[39] A. Dechant, Multidimensional thermodynamic uncertainty relations, J. Phys. A: Math. Theor. **52**, 035001 (2018).
[40] See Supplemental Material at http://link.aps.org/supplemental/10.1103/PhysRevResearch.6.L022044 for details on the calculation of currents, diffusion coefficients, and correlation; the linear response regime; the full hydrodynamic calculations; the intuitive meaning of $\theta_{\beta\alpha}$; and results for negative chemical affinity.
[41] U. Seifert, Stochastic thermodynamics, fluctuation theorems and molecular machines, Rep. Prog. Phys. **75**, 126001 (2012).
[42] P. Hänggi, P. Talkner, and M. Borkovec, Reaction-rate theory: fifty years after Kramers, Rev. Mod. Phys. **62**, 251 (1990).
[43] B. Derrida, Velocity and diffusion constant of a periodic one-dimensional hopping model, J. Stat. Phys. **31**, 433 (1983).
[44] Z. Koza, General technique of calculating the drift velocity and diffusion coefficient in arbitrary periodic systems, J. Phys. A: Math. Gen. **32**, 7637 (1999).
[45] The vanishing of J at large force can be understood mechanistically in the context of the three-sphere microswimmer. This feature is caused by the swimmer stalling into one of its four internal states: no matter on which sphere and in which direction the external force is applied, there is always a state transitioning out of which (both toward the next or the previous state in the cycle) requires that the sphere move against the external force acting on it.
[46] R. K. P. Zia, E. L. Praestgaard, and O. G. Mouritsen, Getting more from pushing less: Negative specific heat and conductivity in nonequilibrium steady states, Am. J. Phys. **70**, 384 (2002).
[47] O. Bénichou, P. Illien, G. Oshanin, A. Sarracino, and R. Voituriez, Microscopic theory for negative differential mobility in crowded environments, Phys. Rev. Lett. **113**, 268002 (2014).
[48] While the full expression of the TUR in linear response was derived in the seminal Ref. [17], this particular consequence appears to have been overlooked.
[49] R. Bebon, J. F. Robinson, and T. Speck, Thermodynamics of active matter: Tracking dissipation across scales, arXiv:2401.02252.